

# An open-pit coalmine surcharged by artesian water pressure

**Marta Dolezalova**, Dolexpert – Geotechnika, Prague, Czech Republic

**Ivo Hladik**, Dolexpert – Geotechnika, Prague, Czech Republic

**Vlasta Zemanova**, Dolexpert – Geotechnika, Prague, Czech Republic

**ABSTRACT:** The Jiri Open-Pit Coalmine, with its highly productive coal measure, is located in a protected region of the Czech Republic that is famous for its spas and artesian thermal springs. A pressurized aquifer underlies the mine. The mining advance is limited by the hazard of potential hydraulic fracturing and resultant flooding of the mine, as well as by serious changes to the hydrogeological conditions of the whole region. To prevent this hazard, the aquifer pressure has been reduced by drainage wells. Between 1976 and the present time, estimates were made of the feasibility of the mining advance at a minimum pressure head reduction, i.e. for the minimum environmental impact. An interactive procedure has been applied using numerical models calibrated according to field measurements, and a monitoring system updated according to the numerical models. The paper describes the predicted and observed performance of the mine in safe and critical conditions, the estimated failure mechanisms and the hydraulic fracturing incidents that have occurred, as well as different approaches used to assess the hydraulic fracturing hazard in various mining conditions.

**KEYWORDS:** Open-pit coalmine, pressurized aquifer, hydraulic fracturing hazard, safety assessment, interactive use of monitoring and modeling, finite element application

## INTRODUCTION

The paper describes the solution to the complex problems of environmental geotechnics, hydrogeology, and mining of the Sokolovsko Coalfield. This coalfield, with its highly productive coal measure, is located near Karlovy Vary, a well-known spa region of the Czech Republic famous for artesian thermal springs (Figure 1). A pressurized aquifer underlies the open-pit coalmines, which limits mining advances because of the potential for hydraulic fracturing. Should hydraulic fracturing occur, mines could flood, with serious consequences to the hydrogeological conditions of the whole region.

The paper focuses on the case history of the Jiri Mine (Figure 2), which is noted for a highly productive, good-quality coal measure which is planned to be continuously operated up to 2030. Due to overburden removal (70-170 m), there is substantial unloading of the 50 m to 60 m thick protective rock barrier composed of practically impervious tuffaceous claystone (Figure 3). If the aquifer water pressure were to exceed the minor principal stress and tensile strength of the rock barrier along the confining boundary, hydraulic fracturing could occur. To prevent the hydraulic fracturing hazard, the aquifer pressure head has been reduced by drainage wells. Between 1976 and the present time, estimates were made of the feasibility of the mining advance at a minimum pressure head reduction, i.e. for the minimum environmental impact. A long-term interactive procedure involving numerical models calibrated according to field measurements and a monitoring system updated according to the numerical models was applied. The procedure is an application of the observational method that was introduced by Terzaghi and Peck (Peck, 1969). It provides authorities with reliable input for decision-making, which results in a more effective control of mining advance.

The feasibility of open-pit mining in given conditions depends on a number of factors (depth of the mine bottom, thickness of the rock barrier, occurrence and character of tectonic faults, and permeability of aquifer strata), which vary as the mine advances. Accordingly, three characteristic periods of the mining advance are distinguished: a relatively safe period up to 1990, a critical period with maximum depth of mining up to 2000, and the current stage, which is influenced by a major tectonic fault, the Grasset Fault.

During the initial period of relatively safe mining (1976-1990), the measurement results were back analyzed in order to select a proper constitutive model and parameters for materials. Using a 2-D Finite Element Model (FEM), the possible failure mode of the rock barrier was predicted. Due to large horizontal stresses, there is not much probability of the barrier

Dolezalova, M., Hladik, I., Zemanova, V. (2006), *An open-pit coalmine surcharged by artesian water pressure*, International Journal of Geoengineering Case histories, <http://casehistories.geoengineer.org>, Vol.1, Issue 1, p.35-55.

cracking by bending, as it has previously been assumed. Instead, opening of flow paths along the faults and seams reducing the impermeability of the rock barrier could occur. Such critical situations occurred during the second period of mining (1991-1999) when the mine reached the maximum depth. Occasional rupture of casings of wells crossing the rock barrier took place, which caused temporary pressure drop in the aquifer. The reasons for these incidents and the related failure mechanism were later identified by coupled 2-D UDEC (ITASCA, 1993) simulations, which matched well with the observations.

Monitoring of the hydrogeological conditions of the rock barrier has been proposed and large coupled 3-D FEM models, which conformed to the geometry of the mine and configuration of the faults, were performed. The 3-D models predicted hydraulic fracturing hazard along a large tectonic fault (the Grasset Fault) being approached by the mine (Figure 4). Local water pressure head reduction and other measures were recommended, but unfortunately, they were not fully implemented. In 2000 the mine reached the Grasset Fault and due to local imbalance of the fluid pressure and rock pressure, some accidents occurred. In order to cope with this new situation, a refined approach to the safety assessment was elaborated using 2-D parametric studies to reflect the varying aquifer permeability and to evaluate the influence of this factor. To gain a better insight into the problem, an accident bringing about leakage of thermal water from the aquifer was carefully simulated. Based on this analysis and a series of new 2-D models, monitoring of the fault and protective measures ensuring safe mining along the Grasset Fault were recommended. All these activities and the current situation at the mine are outlined in the paper.

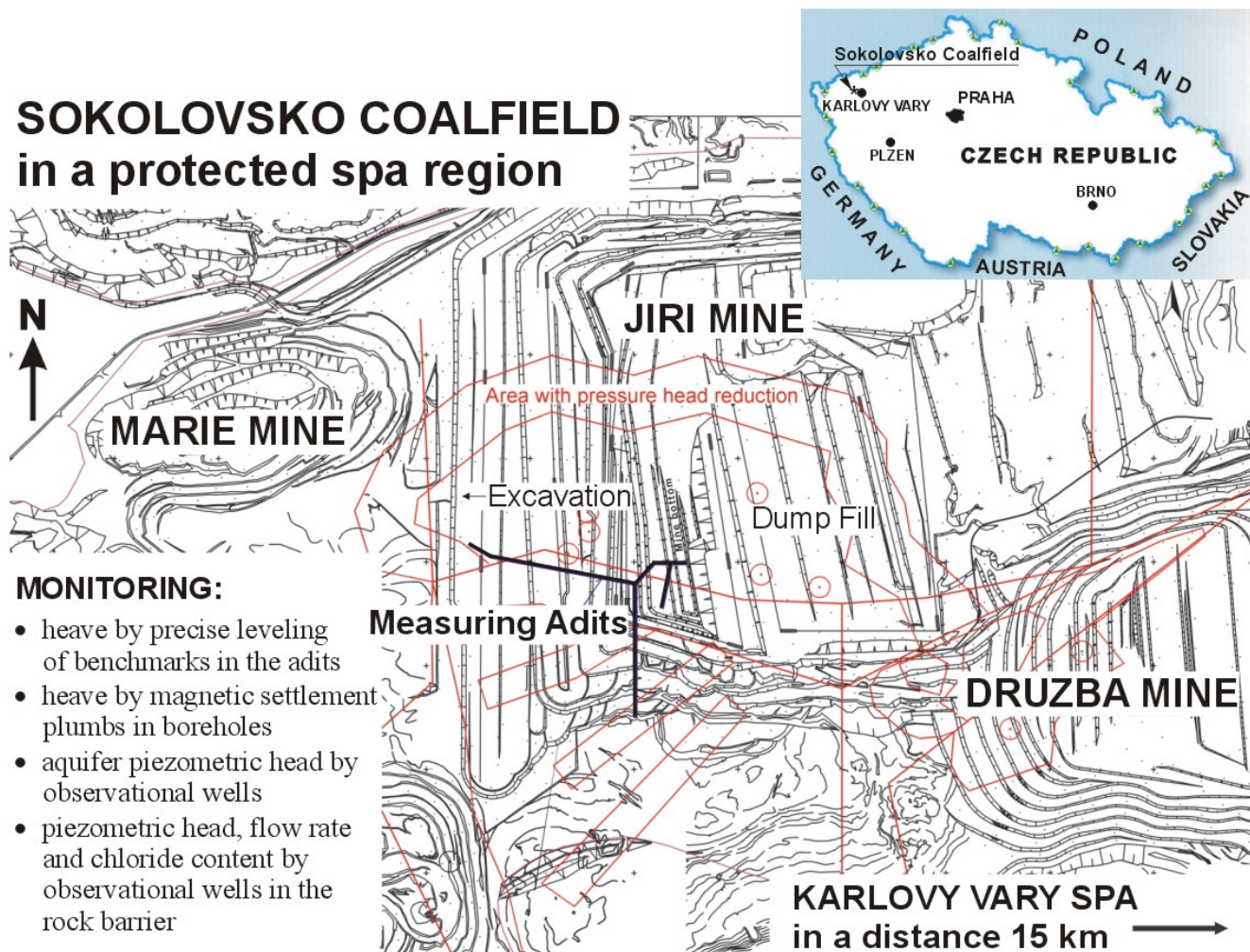
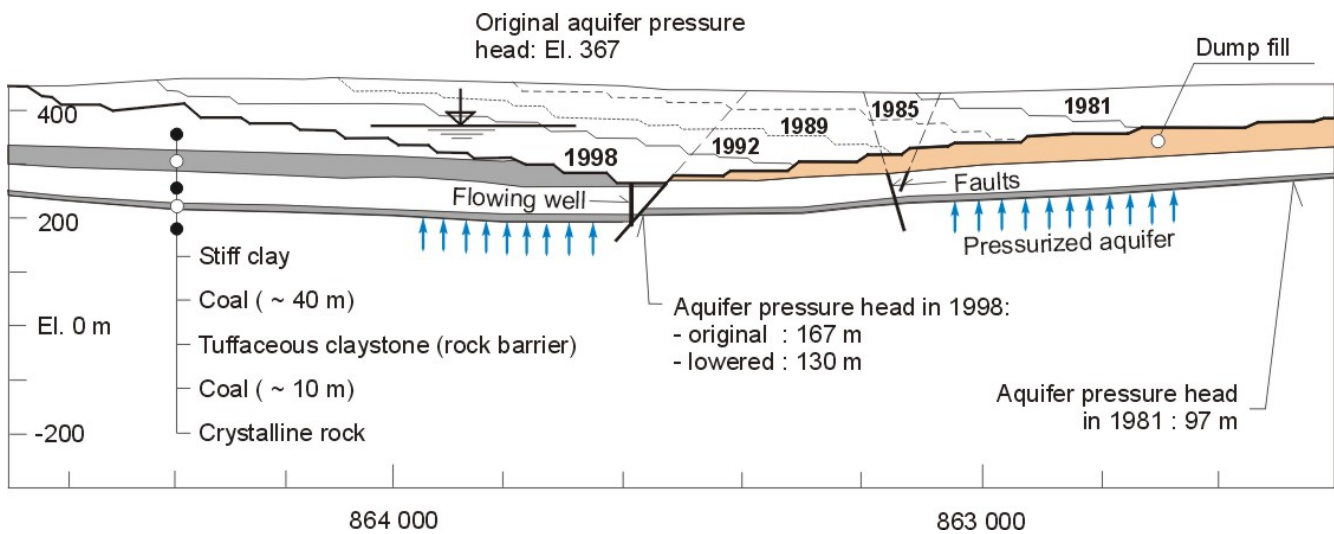


Figure 1. Layout of Jiri Mine with monitoring adits excavated along the bottom of coal seam.



Figure 2. View of the Jiri Mine in 2004 (Vobornikova, 2004).





*Figure 4. View of the upper part of the Grasset Fault (Vobornikova, 2002).*

## BACKGROUND INFORMATION

### Description of the Mine

The Jiri Open-Pit Coalmine has operated since 1960. Owing to a thick coal seam of good quality (sulphate content below 1%, thickness up to 50 m) the mine is one of the most economically attractive facilities of Sokolovsko Coalfield (Figure 5). The layout of the mine and the measuring adits is shown in Figure 1. Mining advances in the east–west direction with a rate of about 100 m in a year. The excavation front is about 2 km and the width of the mine bottom, kept as small as possible, does not exceed 100-150 m (Figure 3).

Figure 3 shows a typical cross section displaying the mining advance and the characteristic geological and hydrogeological conditions around the mine. Crystalline rock, sandstone and a thin coal seam form the artesian water-bearing stratum. The pressure aquifer is confined by tuffaceous claystone, which combined with a clayey coal stratum form an impervious rock barrier of 50 m to 60 m thick. This stratum is overlain by 70 m - 170 m of overburden, which includes a basal 50 m thick upper coal seam covered by stiff fissured clays.

### Site Characterization

In situ tests of rock mass in an exploratory adit and laboratory tests of rock material were carried out (Hudek et al. 1986) to investigate the deformation, strength characteristics, and other properties of the volcanic-detrital tuffaceous claystone (35 in situ tests and 187 laboratory tests) and xylitol-detrital coal seams (17 in situ tests and 49 laboratory tests). Large-scale samples (0.5 m x 0.5 m x 1.0 m) of the tuffaceous claystone and coal before and after testing are shown in Figures 6-9. The main results of the tests are summarized in Table 1. The symbols denote unit weight  $\gamma$ , initial moduli at loading  $E_{in}$  and

unloading  $E_{unl}$ , Poisson's ratio  $\nu_{in}$ , cohesion  $c$ , friction angle  $\phi$ , and tensile strength,  $\sigma_t$ . The term "Faults (1)" refers to the faults in the tuffaceous claystone and "Faults (2)" refers to those in the coal seam.

The hydraulic transmissivity and storativity of the upper part of the aquifer strata (granite, sandstone and the lower coal seam) were determined by pumping tests (Pazdera and Vobornikova, 1992) and used to evaluate coefficients of permeability. A summary of hydraulic properties of the aquifer strata, including crystalline rocks of varying permeability (permeable granite and almost impermeable metamorphic granite) is given in Table 2.

According to the observational well records, the aquifer piezometric head before mining was at El. 367 m above the sea level. To make the mining advance possible, since 1989 the pressure head has been gradually reduced via drainage wells and reached El. 342 in 1993, El. 332 in 1996 and El. 329 in 1998. Nowadays, the piezometric head is at El. 330 to El. 333 in the central part of the mine and at El. 323 along the Grasset Fault.

The components of the in situ geostatic stress state of the region before mining were determined by the overburden self-weight in the vertical direction and by the lateral pressure coefficient at rest  $K_0$  in the horizontal direction. A possible range of  $K_0 = 0.6 - 0.8$ , which was important for assessing the hydraulic fracturing hazard, was found in an indirect way, by back analyzing the measured heave of the mine bottom (Dolezalova, 1986).

The feasibility of open-pit mining in given conditions depends on a number of factors (depth of the mine bottom, thickness of the rock barrier, occurrence and character of tectonic faults, permeability of aquifer strata), which vary as the mine advances. Accordingly, three characteristic periods of the mining advance are distinguished: a relatively safe period up to 1990, a critical period with deepest altitude of mining up to 2000 and the current stage influenced by the Grasset Fault.



Figure 5. Jiri Mine - view of the 50 m thick coal seam (Vobornikova, 2000).

Table 1. Deformational and strength characteristics of rock units.

| Material             | Numbers in Figure 17 | $\gamma$<br>kN/m <sup>3</sup> | $E_{in}$<br>MPa | $E_{unl}$<br>MPa | $\nu_{in}$ | $c$<br>MPa | $\phi$<br>degrees | $\sigma_t$<br>MPa |
|----------------------|----------------------|-------------------------------|-----------------|------------------|------------|------------|-------------------|-------------------|
| Tuffaceous Claystone | 3, 10                | 22.7                          | 200             | 1400             | 0.25       | 0.27       | 28.3              | 0.20              |
| Faults (1)           | 18                   | 19                            | 90              | 600              | 0.25       | 0.10       | 19.4              | 0.06              |
| Coal                 | 6, 8                 | 11.9                          | 170             | 550              | 0.20       | 0.18       | 30.5              | 0.06              |
| Faults (2)           | 22                   | 11.9                          | 80              | 300              | 0.20       | 0.06       | 30.5              | 0.03              |

Table 2. *Hydraulic properties of the aquifer strata.*

| Material            | Numbers<br>in Figure 17 | Transmissivity<br>m <sup>2</sup> /sec | Storativity m <sup>2</sup> /sec | Permeability<br>m/sec    |
|---------------------|-------------------------|---------------------------------------|---------------------------------|--------------------------|
| Sandstone           | 12                      | $10^{-5}$ to $10^{-3}$                | $10^{-5}$ to $10^{-3}$          | $2.10^{-6}$ to $10^{-4}$ |
| Coal                | 6, 8                    | $10^{-5}$ to $10^{-3}$                | $4.10^{-5}$ to $10^{-3}$        | $6.10^{-6}$ to $10^{-5}$ |
| Granite             | 1 (alternative)         | $3.4 \times 10^{-5}$                  |                                 | $1.7 \times 10^{-6}$     |
| Metamorphic Granite | 1                       | $7.5 \times 10^{-7}$                  |                                 | $1.7 \times 10^{-8}$     |



Figure 6. Block of the tuffaceous claystone (0.5 m x 0.5 m x 1.0 m) prepared for an in situ triaxial compression test (Hudek, 1986).



Figure 7. Part of the failed block of the tuffaceous clavstone after testing (Hudek 1986)



Figure 8. Blocks of coal prepared for in situ triaxial compression tests (Hudek, 1986).



Figure 9. Failed block of coal after testing (Hudek, 1986).



---

## MINING ADVANCE IN SAFE CONDITIONS UP TO 1990

In the 1970s and 1980s the mine bottom deepened by about 70 m (from El. 370 m to El. 300 m, Figure 3), but the load of the thick rock barrier always exceeded the aquifer pressure along the confining boundary. Furthermore, since competent rock with few sporadic faults formed this part of the barrier, no rock pressure/fluid pressure imbalance that could cause hydraulic fracturing hazard could occur and this is considered the safe period of mining.

### Interactive Process Between Monitoring and Modeling

During the safe period, methods and tools were developed to allow solution of the anticipated problems of mining in the future critical region. To assess the effect of unloading on the rock barrier (due to excavation of the maximum overburden) and to find the optimum pressure head reduction, almost all existing methods for solving rock mechanics problems (analytical solutions, physical models, field measurements, and numerical methods) were examined. While most methods predicted well the necessary pressure head reduction, they failed to estimate the expected deformation. At the conclusion of the research, a strategy for interactive use of monitoring and numerical models emerged as the best approach for checking the feasibility of the mining advance and safety of the mine.

The interactive process started as a pure prediction using 2-D FEM (Dolezalova et al. 1977). Maximum heave of the unloaded mine bottom of about 0.80 m was predicted, instead of the 7.0 m estimated by early physical models from equivalent materials that were subjected to incorrect loading/unloading sequences (Filip, 1975).

To solve this problem and gain insight on the feasibility of the planned mining advance, extensive monitoring of the mine bottom heave over a large area was proposed and performed. Benchmarks at intervals of about 25-30 m were installed in the adits along the coal seam bottom for a length of more than 3 km (Figure 1). Precise leveling of the benchmarks was carried out four times a year and the results confirmed the above FEM prediction, i.e. that excavation of a 10 m thick layer induces heave no more than 0.03 - 0.05 m. In order to investigate the distribution of the measured heave inside the rock barrier, magnetic settlement plumbs in boreholes were installed.

The hydrogeological conditions were monitored by observational wells in the aquifer (piezometric head, temperature and chemical constituents of thermal water) and in the rock barrier (temperature, chemical constituents and flow rate). Measurements of the rock barrier behavior allowed checking of possible structural changes within the barrier as predicted by the numerical models.

During the last 30 years, the monitoring system was updated several times to add or change a component of the equipment such as GPS, remote records, etc. However, the types of measured data (heave at the bottom of the rock barrier, heave on the mine bottom surface, distribution of heave with depth, aquifer piezometric head, etc.) remained without changes and formed continuous time dependent series of data providing a highly valuable database for calibrating the numerical models.

### FEM Code and Constitutive Model

A modified version of the original CRISP FEM Code (Britto and Gunn, 1987) called CRISP-PATH was used for most of the solutions presented below. The modified version has been developed since 1993, extending the capabilities of CRISP to several new areas of application, especially to solutions of larger 3-D problems and to appropriate constitutive modeling. Along with a number of advanced constitutive models, highly efficient solvers of arising linear and nonlinear systems of equations, namely linear iterative solvers (Hladik et al. 1997) and non-linear solvers of Newton type (Hladik, 1998) were implemented. These made possible the solution of large 3-D problems with complex geometry, loading sequences, and material behavior as presented below.

A non-linear, path-dependent constitutive model (which accurately describes the deformation response of geomaterials in the pre-peak regime) was used (Dolezalova, 1991). According to this model, the stiffness of the material response depends not only on the stress level, but also on the incremental changes in the direction of stress path. These are determined by average normal stress level increase/decrease and by relative shear stress level increase/decrease at stress points. A variable stiffness approach is used in the pre-peak regime and a non-associated perfectly plastic approach with Mohr-Coulomb failure surface is used in the peak regime. In this way the function of much more sophisticated elastic-plastic double hardening models is approximated. The basic parameters like  $E_p$ ,  $E_{unl}$ ,  $c$ ,  $\phi$  were determined based on the in

situ tests (Table 1), and only the exponents describing their change with the normal and shear stress level were calibrated based on the measured heave. Figure 10 depicts the results of such a trial-and-error fitting procedure that were carried out for four years and for more than 100 benchmarks. The calibrated set of parameters has been used without any changes since 1991. Details of the constitutive model and the parameters that were used are given in the Appendix.

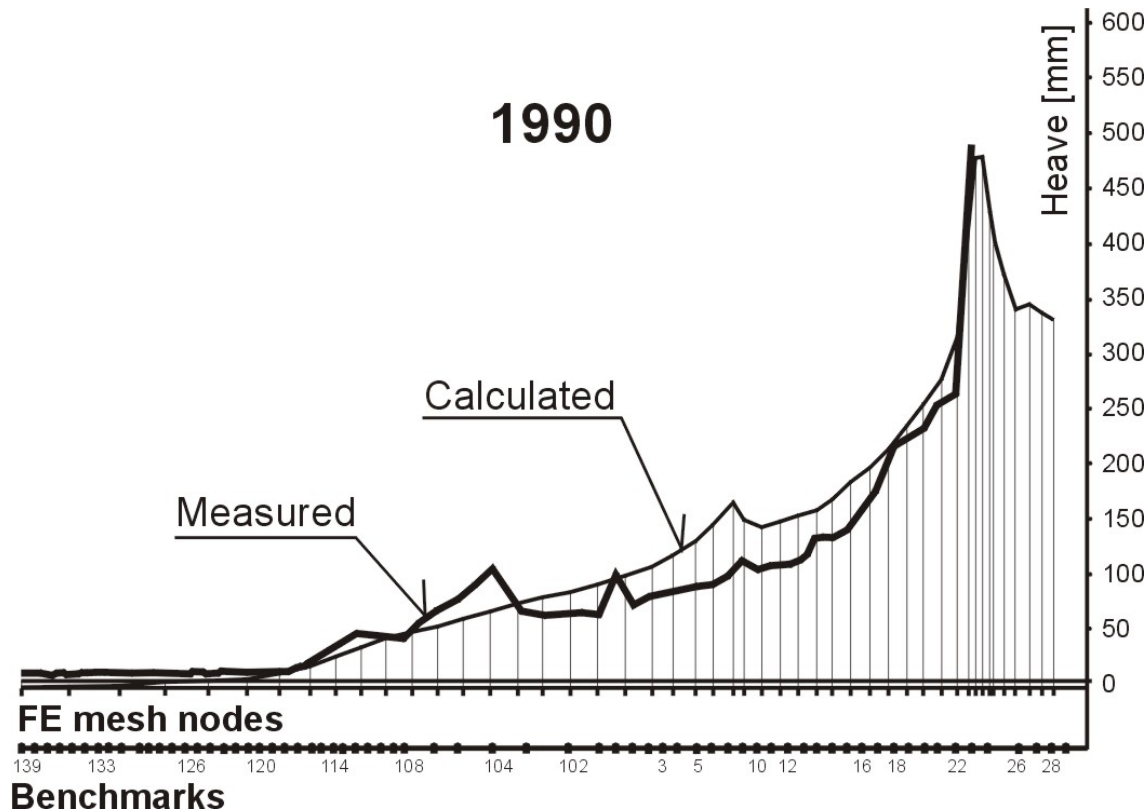


Figure 10. Heave of the rock barrier as measured in the adits and back analyzed by FEM.

## MINING ADVANCE IN CRITICAL CONDITIONS UP TO 2000

In the 1990s, the mine deepened by another 40 m (from El. 300 m to El. 260 m, Figure 3) and the weight of the rock barrier no longer exceeded or balanced the initial aquifer pressure along the confining boundary. Furthermore, as mining advanced to higher depths, more and more tectonic faults were encountered, which disrupted the barrier. The strike directions of the faults were perpendicular to the direction of the mining advance at the beginning of the period, but became more variable and complex towards the end of it. Highly permeable rocks formed the water bearing strata in this part of the aquifer, which allowed for efficient water pressure reduction by drainage wells.

### Assessment of Hydraulic Fracturing Hazard

The initial step required for the prediction of the necessary water head reduction for a given mining situation was to introduce criteria quantifying the hydraulic fracturing hazard in the domain. To determine the safety factor against hydraulic fracturing in different directions, the components of the total stress tensor ( $\sigma_x$ ,  $\sigma_y$ ,  $\sigma_z$ ,  $\sigma_{\min}$ ) computed for the rock barrier were related to the aquifer pressure  $p$ . To get a better insight into the problem, different criteria were considered that either included or excluded the tensile strength  $\sigma_t$ . The safety factors including  $\sigma_t$  are as follows:

$$s_{1t} = (\sigma_x + \sigma_t)/p \quad s_{2t} = (\sigma_y + \sigma_t)/p \quad s_{3t} = (\sigma_z + \sigma_t)/p \quad s_{4t} = (\sigma_{\min} + \sigma_t)/p$$

In these relations,  $s_{1t} < 1$  and  $s_{3t} < 1$  along the confining boundary indicate hydraulic fracturing and flow from the aquifer via vertical fractures controlled by horizontal stresses  $\sigma_x$  and  $\sigma_z$ . A factor  $s_{2t} < 1$  indicates horizontal hydraulic fractures

controlled by the vertical stress component  $\sigma_y$ . Hazard due to fractures in the least resistant direction is determined by  $s_{4t} < 1$  controlled by the minor principal stress component  $\sigma_{min}$ .

To simplify the stress analysis, perfectly permeable aquifer and impermeable rock barrier were assumed and a contact layer along the confining boundary was introduced to simulate the joint opening/closure in the aquifer. The characteristics of this layer were calibrated based on field measurements. 2-D mechanical models were initially implemented and were subsequently enhanced by 2-D and 3-D coupled mechanical-hydraulic models.

### Ruptures of Flowing Well Casings and UDEC Simulation

Stress analysis using 2-D FEM discovered the unfavorable influence of tectonic faults, the possible imbalance of the rock pressure, and fluid pressure near them and that the hydraulic fracturing hazard is considerably larger in the horizontal direction than in the vertical one. Accordingly, the possible failure mode of the rock barrier is not cracking by bending, as predicted by early physical models. Instead, progressive hydraulic fracturing along the faults and seams and opening of flow paths occur, which result in reduction of the impermeability of the rock barrier.

Such critical situations have already occurred, because the water pressure reduction by flowing wells has been limited by the limits of the withdrawal from the aquifer. The observed failure mode of the rock barrier was, however, somewhat different from the predicted one. Occasional rupture of casings of wells occurred at a depth of 20 - 30 m, only small springs were observed and about 0.035 m heave of the mine bottom was measured. Other than the first instance of casing rupture when the damage to the well was detected too late, quick application of packers and grouting of the ruptured boreholes has prevented the pressure drop of the aquifer.

An attempt was made to model the first instance of casing damage making use of the capabilities of the UDEC code (ITASCA, 1993) accounting for the structure of jointed rock, fracturing of joints, fluid flow through fractures, grouted bolts for modeling the grouted double casing of wells, etc. In order to account for frequent parallel faults, a 2-D model in longitudinal direction was formulated (Figure 11) and to simplify the solution, steady flow was assumed. In order to compensate for the effect of neglecting slopes of the mine in the longitudinal 2-D model, the contact layer along the confining boundary was strengthened. A number of computed quantities was consistent with the observed ones: 12 m pressure drop, well casing rupture at a depth of 20-25 m, and separation of about 0.07-0.3 m.

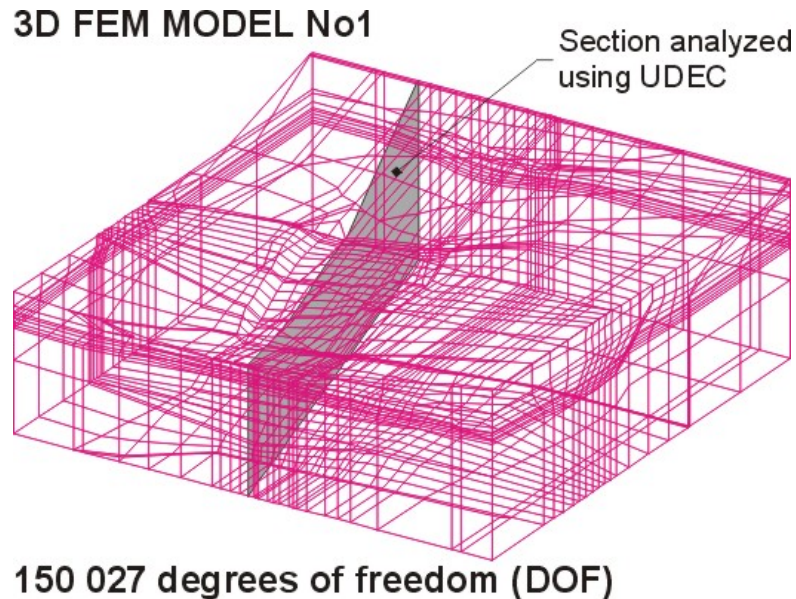


Figure 11. 3D FEM Model No 1 simulating the deepest part of the mine and the longitudinal section analyzed using UDEC.

The results shown in Figures 12a, b, c and d helped to clarify the possible process of borehole rupture. Due to excavation between 1993 and 1995, fractures along the planes of weakness occurred and the rock and fluid pressure imbalance initiated fluid flow from the aquifer. Once the fluid pressure in the horizontal fracture was larger than the overburden weight, rupture

of the well occurred since it was a stiff element in the jointed rock. The last water pressure records registered just before the borehole ruptured confirmed this finding. Apart from that, the modeled scenario differed conservatively from the magnitude and rate of the events resulting in casing damage. In contrast to the model predictions, pressurized water actually accumulated along some clay/coal contacts due to long-term filtering along the faults and not due to fractures along them. The affected areas were smaller and the borehole rupture resulted in a new state of equilibrium, which stopped the process. Therefore, installing a packer in the borehole and loading the area by fill could stabilize the situation.

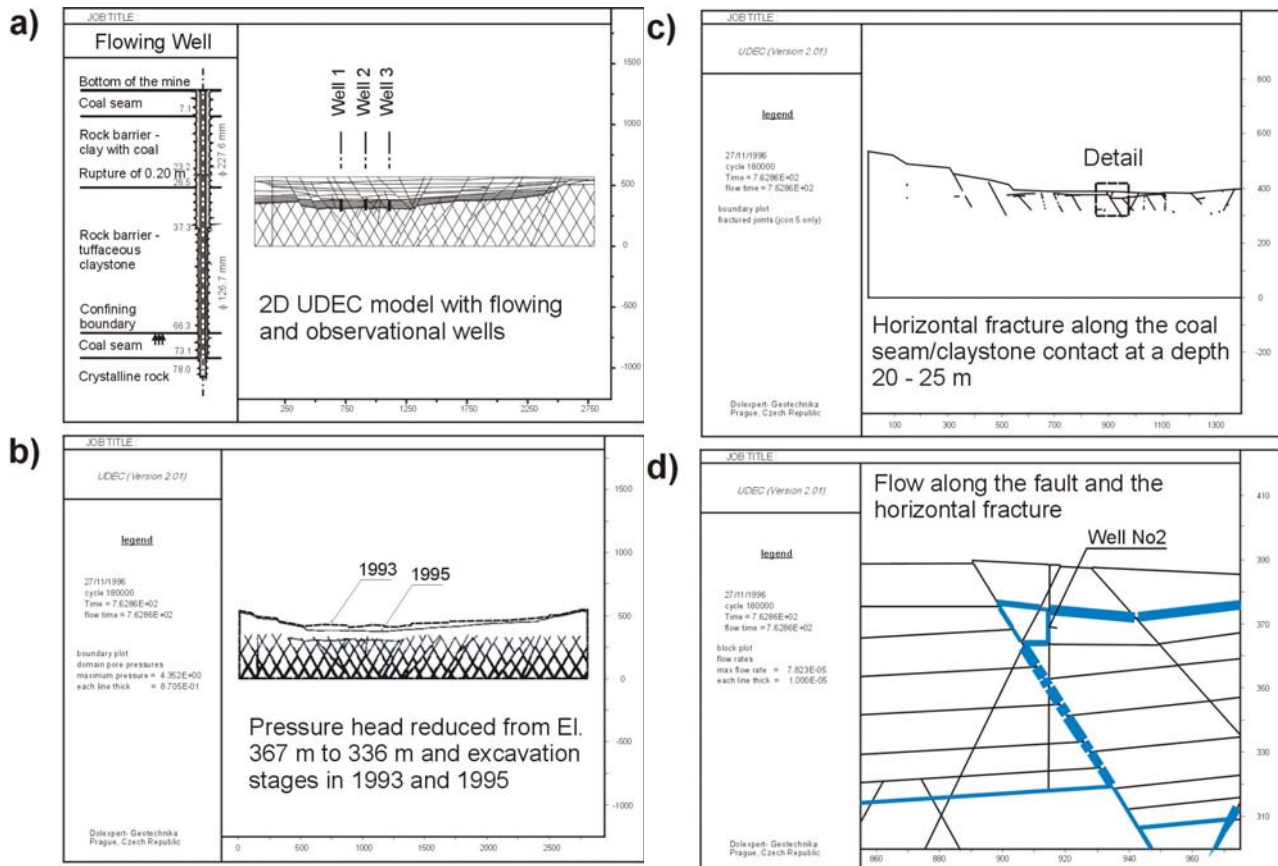


Figure 12. Borehole casing rupture - results of the UDEC analysis.

### 3-D FEM Model of the Deepest Part of the Mine

To cope with the increasing complexity of the geometry of the mine and the configuration of faults, large coupled 3-D FEM models have been developed and implemented since 1998. The first model was developed for decision-making purposes of the Health Department and Mining Authorities concerning the mining advance in 2000. The 3-D model is shown in Figure 11 and some of the results in Figures 13, 14 and 15. To model a proper initial state, the mining advance over the preceding 10 years was carefully simulated. The model was validated by the measurements corresponding to mining advances between 1996 and 1999 without any calibration (Figures 13, 14). The comparison of Figure 15 illustrates how the rock barrier heave, as registered by magnetic plumbs in the MJ1 Borehole (Figure 14), approaches the FEM prediction. A gradual decrease of the initial difference caused by different starting points of measuring and modeling can be observed. The increment of the heave between the top and bottom of the barrier was only 50 mm to 60 mm, i.e. only 10 % of the total heave of 300 mm to 600 mm. This result suggests that the remaining 90% of the heave is due to joint opening in the aquifer. According to this finding, the structural changes of the barrier due to unloading are not so dramatic as predicted. Also, the simulation of the joint opening in the aquifer by a contact layer is an acceptable approximation.

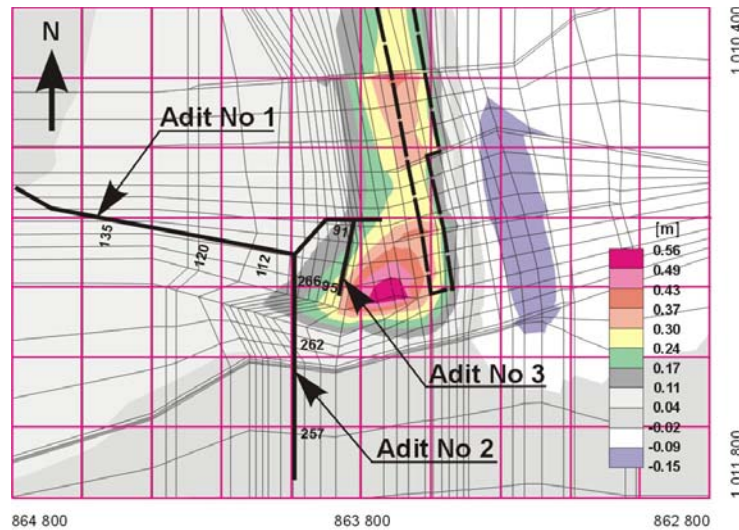


Figure 13. Heave of the rock barrier due to excavation in 1996 - 1999 calculated by the 3D FEM Model No 1.

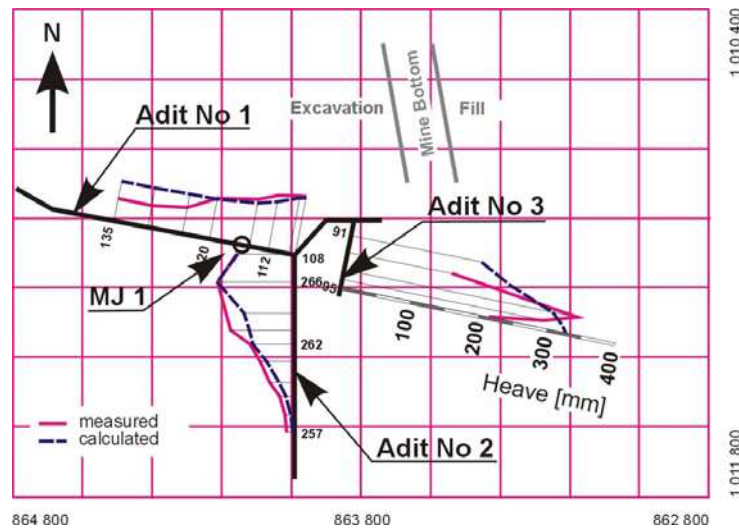


Figure 14. Comparison of calculated and measured heave along the adits from 1996 to 1999.

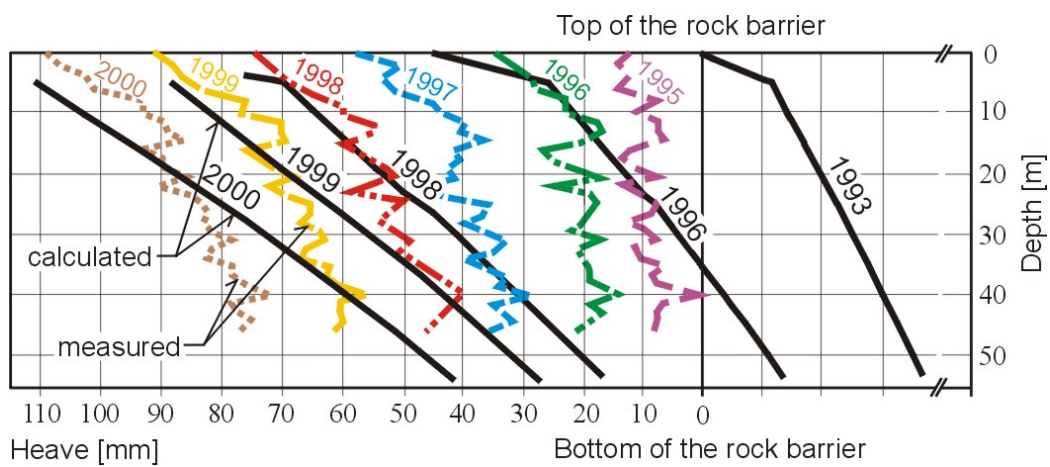


Figure 15. Comparison of the rock barrier heave measured by magnetic settlement plumb.

## MINING IN CURRENT CONDITIONS ALONG THE GRASSET FAULT

In 2000, the Jiri Mine advanced into a region with new geological and hydrogeological conditions. First, permeable granite forming the water-bearing strata changed to a more or less impermeable metamorphic granite, which complicated the reduction of pressure head by the drainage wells. Second, the mine reached the Grasset Fault (Figure 4 and 16), which dislocated the strata and divided the coalfield into two parts: the lower part with a confining boundary to the aquifer at El. 210 m; and the upper part with a confining boundary at El. 270 m. Between these parts, different strata with varied permeabilities form the confining boundary of the aquifer. The layout of the fault is shown in Figure 16. The most problematic geology is shown as cross section A – A' in Figure 17.

The abrupt geological changes brought changes in the mining conditions. From one point of view, the high-quality coal measure located close to the surface and the lower aquifer pressure due to the higher altitude facilitated the mining advance. From the other point of view, part of the confining boundary along the fault was surcharged and protected only by a low-density coal seam instead of a competent tuffaceous claystone stratum (Figure 17). This enhanced the hydraulic fracturing hazard induced by mining.

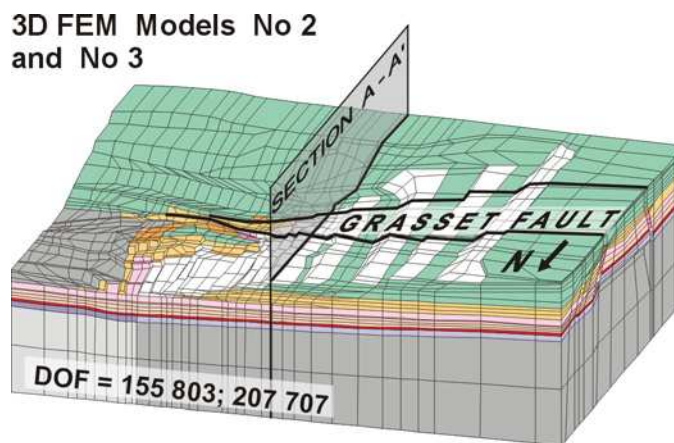


Figure 16. 3D FEM Models No 2 and No 3 simulating Grasset Fault and the longitudinal section A - A' analyzed by 2D FEM.

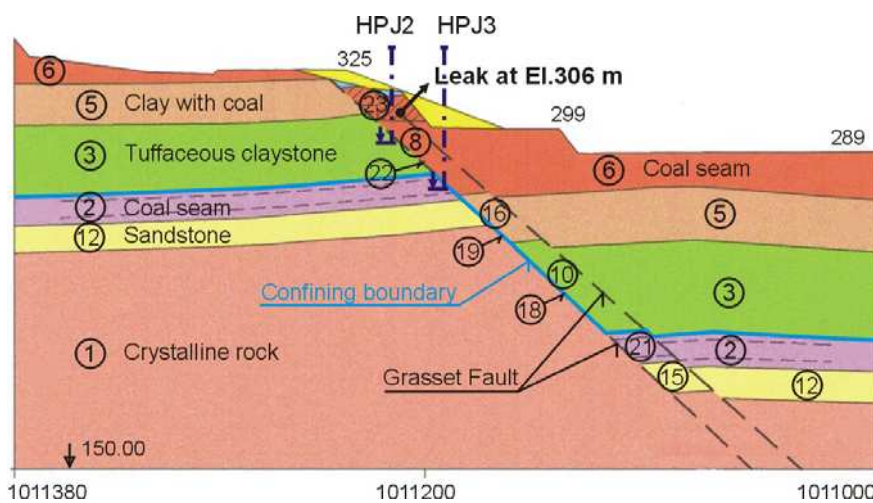


Figure 17. Geological conditions and mining advance along the Grasset Fault (Cross section A - A').

## Mining Along the Grasset Fault and Analyses Assuming Perfectly Permeable Aquifer

The above complex conditions were incorporated in two new 3-D FEM models (Figure 16). Assuming a perfectly permeable aquifer due to fractures in metamorphic granite, the safety factor  $s_{4t}$  was calculated at different piezometric heads for the mining advance in 2001. Hydraulic fracturing hazard along the confining boundary in the area of the Grasset Fault was predicted at El. 329 m (Figure 18a). A pressure head reduction to El. 320 m (Figure 18b) and a protective pillar of coal left along the fault were recommended. Because mining was taking place at higher elevations and low permeability of rocks in the aquifer was expected, the possible effect of fluid/rock pressure imbalance was underestimated and the recommendations resulting from our numerical analysis have not been accepted. Excavation of smaller blocks of coal near the fault caused two unanticipated leaks from the aquifer at the higher mining level at El. 306 m. Fortunately, loading by fill of the nearby area stopped one leak and reduced the other. To simulate and evaluate these events, an improved approach to assess hydraulic fracturing hazard along the confining boundary of the aquifer was necessary.

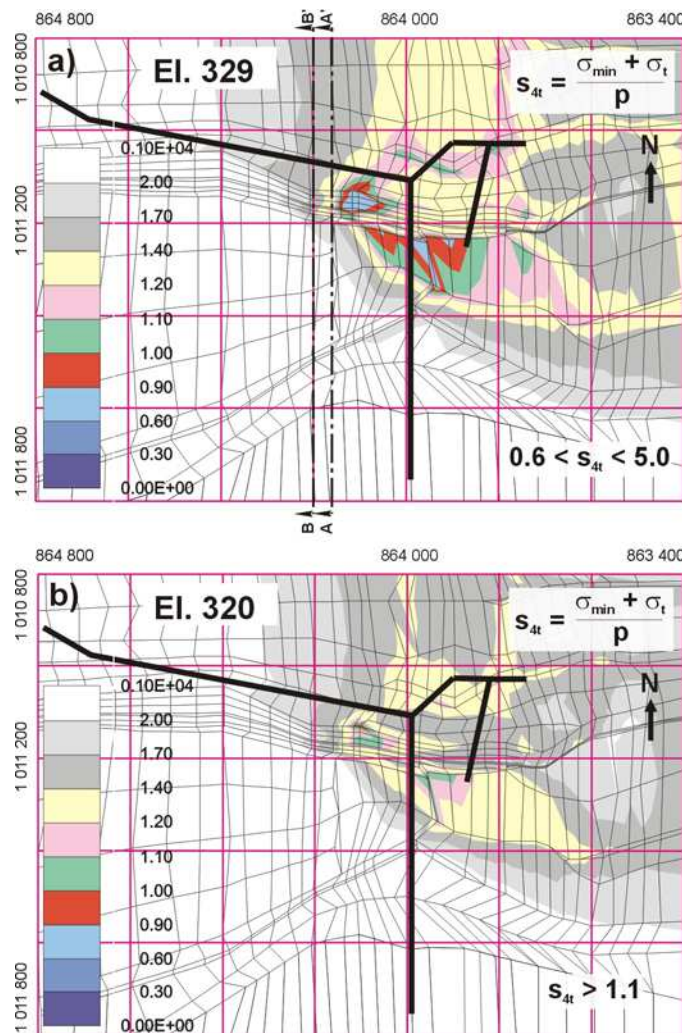


Figure 18. Safety factor against hydraulic fracturing  $s_{4t}$  along the Grasset Fault at piezometric heads (a) El.329 m and (b) El.320 m.

## Modeling of Pressure-Dependent Fluid Flow through the Confining Boundary of the Aquifer

An attempt was made to simulate flow from the aquifer through the confining boundary into the domain above the confining boundary in the event that hydraulic fracturing occurs. An algorithm was implemented into the CRISP-PATH FEM code. The aquifer and the domain above the confining boundary ('upper domain') is considered a porous, two-phase

medium. The confining boundary of the aquifer is modeled by means of a thin layer of impermeable elements. As soon as  $s_{4t} \leq 1$  in an element of the confining boundary, the element is set as permeable and a hydraulic connection is established between the aquifer and the upper domain. A time-dependent fluid flow through the confining boundary depends on the permeability and the pore pressure (Biot's consolidation, i.e. a coupled mechanical-hydraulic problem). The initial pressure difference of the aquifer and the upper domain (rock/fluid pressure imbalance) is determined according to the relation  $p - (\sigma_{min} + \sigma_t)$  for the elements of the confining boundary with  $s_{4t} \leq 1$ . The value of the coefficient  $s_{4t}$  along the confining boundary can be checked at each time step of the solution. For  $s_{4t} > 1$  the element is set to be impermeable. For the region of the Grasset Fault a slightly modified safety factor of  $s_{4b} = (\sigma_{min} + \sigma_{tb})/p$  was introduced. That means that only the tensile strength of the competent tuffaceous claystone is considered in the safety calculations.

Using this algorithm, the effect of permeability of the aquifer strata on the safety of mining when fluid/rock pressure imbalance occurs was analyzed. A 2-D parametric study was elaborated for the adjacent cross section B - B' (Figure 18a), where a protective pillar of coal was modeled to shield the fault (Figures 19 and 20). To generate the initial stress state of the section, the 3-D model No 3 was used (Figure 16) and the stress state corresponding to the mining situation in 2000 was transferred from the 3-D model to the 2-D model.

A broader range of coefficients of permeability than those in Table 2 was considered for the strata in the aquifer and those above it. Figures 19 and 20 show results displaying the performance of perfectly permeable aquifer strata ( $k = 1 \text{ m/sec}$ ) and the practically impermeable aquifer strata ( $k = 10^{-8} - 10^{-10} \text{ m/sec}$ ). The pore pressure in the pillar, flow through the fault (flow rate 3 lt /sec), and heave of the domain were calculated for the permeable aquifer (Figures 19a, b). The pressure decrease in the aquifer, the negligible flow through the fault (flow rate 0,1 lt /sec) and settlement of the domain were calculated for the impermeable aquifer (Figures 20 a, b). Admittedly, this is a situation in which the fluid/rock pressure imbalance might have occurred without any hydraulic fracturing. However, the problem is that the aquifer strata are disrupted by fractures and their permeabilities are hence variable. Consequently, it is conservative to assume permeable aquifer strata for safety assessments.

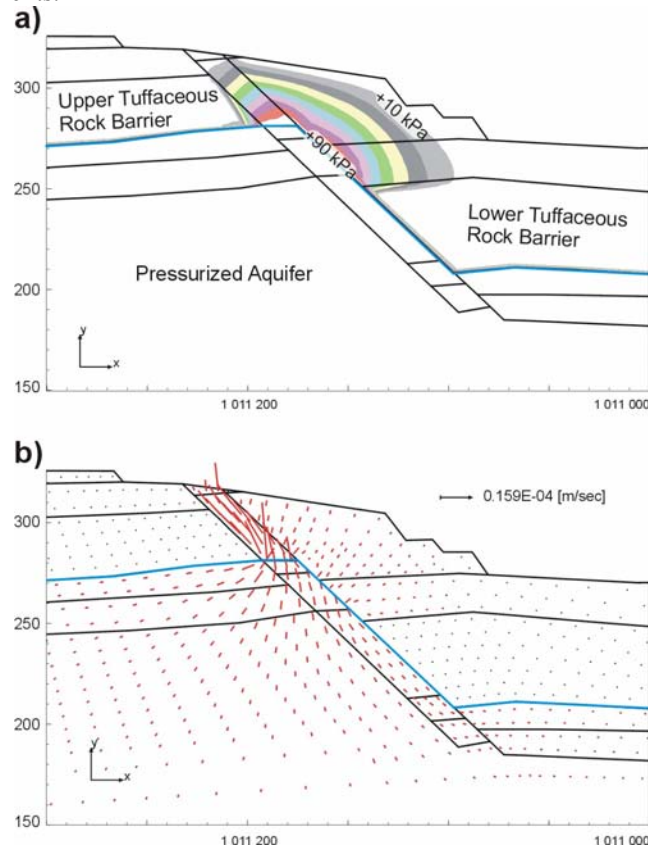


Figure 19. Ideally permeable aquifer (El.325) - pore pressure increase (a) and velocity vectors (b) due to rock/fluid pressure imbalance.

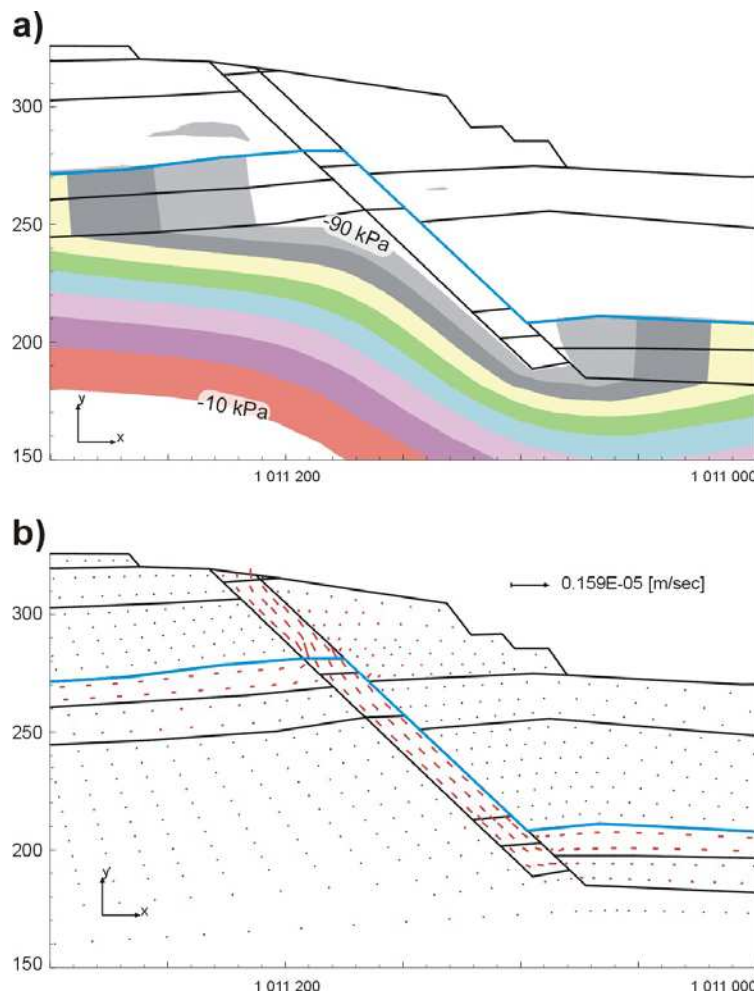


Figure 20. Practically impermeable aquifer (El.325) - pore pressure decrease (a) and small velocity vectors (b) due to rock/fluid pressure imbalance.

#### Hydraulic Fracturing Incident at the Grasset Fault and its Simulation

In January 2003, an attempt to mine the high quality coal near the Grasset Fault in smaller blocks, but at an aquifer pressure which was higher (El. 336 m) than inferred from the model (El. 320 m), resulted in local hydraulic fracturing of the confining boundary. The event was accompanied by fracturing of the fault by pressurized water and the appearance of a leak of thermal water in the most critical area of the mine, as shown in cross section A - A' (Figure 17). The leakage occurred at the relatively high mining level of El. 306 m. The flow rate was about 5 to 6.5 lt/sec.

A detailed hydrogeological investigation of the vicinity of the affected area was carried out. A network of boreholes was drilled to intersect the fault and the piezometric head in the boreholes measured. Pressurized water in the fault and local reduction of the aquifer pressure to El. 312 m in the 20 m x 17 m area of boreholes was observed. Pumping tests of boreholes were performed and the connection of boreholes with the leak investigated. Some of the boreholes (HPJ-2, and HPJ-3) are depicted in Figure 17 and the results of the pumping test are shown in Figure 21. Dewatering of boreholes HPJ-2 and HPJ-5 by pumping, notably reduced the flow rate of the leak, although no similar effect at the remaining boreholes was observed, suggesting heterogeneous permeability of the fault induced by fractures.

Based on the results of the investigation and monitoring, a new 2-D model of the newly established conditions in the mine area of cross section A - A' was created in order to reproduce the incident and understand the causes. The process of excavation and aquifer pressure reduction before and after the incident (i.e. the mining status from December 2000 to

August 2003) was simulated applying the new modeling approach with pressure-dependent permeability of the aquifer-confining boundary (see previous section).

The simulation of the mining status in January 2003, upon completion of the phase of mining in smaller blocks at an aquifer pressure of El. 336 m, revealed the initiation of local hydraulic fracturing for the elements along the confining boundary at areas with safety factor  $s_{4b} \leq 1$ . The values of  $s_{4b}$  were 0.45 between the depths of El. 250 to El. 265 m and 0.60 at El. 278 m. The corresponding initial rock/fluid pressure imbalance between the aquifer and the upper domain was then determined to be 330 kPa.

An attempt was made to determine the 'equivalent' coefficients of permeability  $k$  of the Grasset Fault, which would result in pore pressure distribution and flow rates best fitting the results of the hydrogeological investigation. Given the pressure difference of 330 kPa, a trial-and-error fitting procedure was performed. The 'equivalent' coefficient of permeability of the fractured part of the Grasset Fault was determined to be  $k = 3 \times 10^{-4}$  m/s for materials 18, 19, 22 (i.e., tuffaceous claystone, clay with coal, coal seam in the fault in Figure 17) and  $k_x = 3 \times 10^{-4}$ ,  $k_y = 10^{-5}$  m/s for material 23 (coal debris in the old abandoned mining area in Figure 17), where  $k_x$  and  $k_y$  are the coefficients of permeability in the horizontal and vertical directions. The computed total pore pressures in the aquifer, the Grasset Fault, and the protective coal pillar are depicted in Figures 22a and 22b. The predicted pore pressures are in good agreement with the observed values, namely: a) decreased aquifer pressure reaches El. 312 m, b) pore pressure is at El. 312 m in the upper part of the Grasset Fault up to El. 300 m (borehole HPJ-2); and c) lower pore pressure occurs at El. 306 m near borehole HPJ-3. Corresponding flow vectors are depicted in Figure 23 together with the aquifer permeability coefficients used. The aquifer permeability is here clearly better approximated to the case of a permeable aquifer (Figure 19) than to the case of an impermeable aquifer (Figure 14) as discussed in the previous section. The computed flow through the upper part of the Grasset Fault amounts to 0.0004 m<sup>2</sup>/s per 1 m of the 2-D model width, which for 20 m of the affected area yields a flow rate of 7.8 lt/s. This value is again in agreement with the leakage observed (5 to 6.5 lt/s). The results of the 2-D model clearly supported the hypothesis that the reasons for the incident lie in the occurrence of two events: 1) the rock/fluid pressure imbalance in the upper part of the Grasset Fault; and 2) a sufficiently permeable aquifer strata surrounding the area of this imbalance.

It should be noted that using the above-mentioned boreholes, the leak was successfully sealed by grouting. An important lesson drawn from the incident was that to ensure the safety of the mining operations, a protective coal pillar needed to be left adjacent to the Grasset Fault.

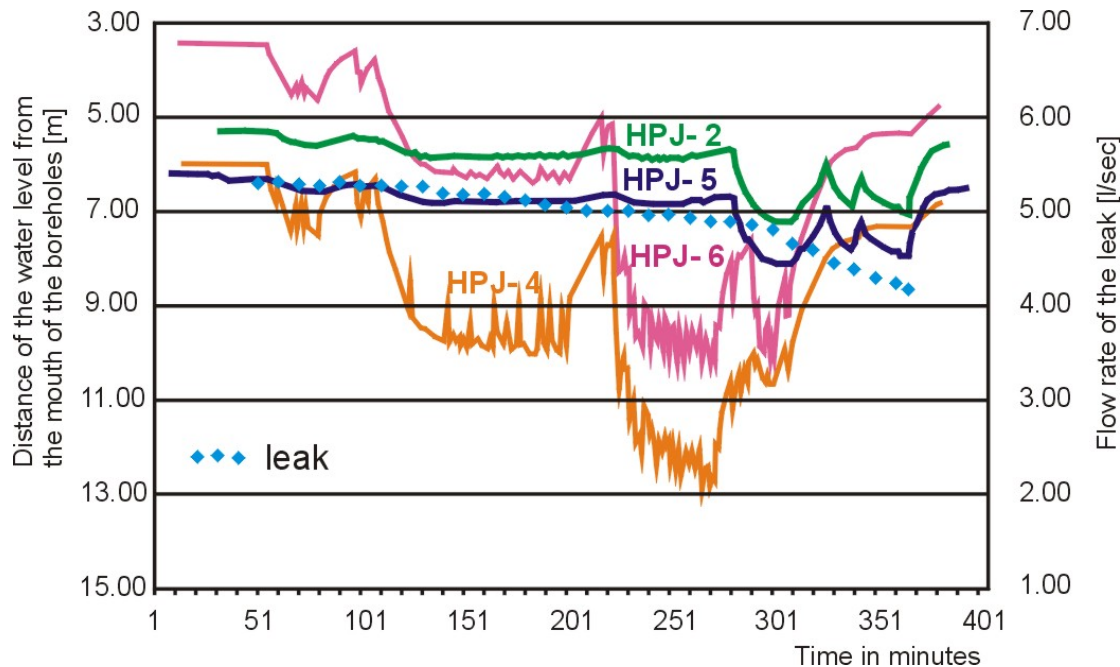


Figure 21. Pumping test of the leak at the Grasset Fault (El.306) – flow rate of the leak and water level decrease/increase in the exploratory boreholes HPJ2, HPJ4, HPJ5 and HPJ6 (Vobornikova, 2003).

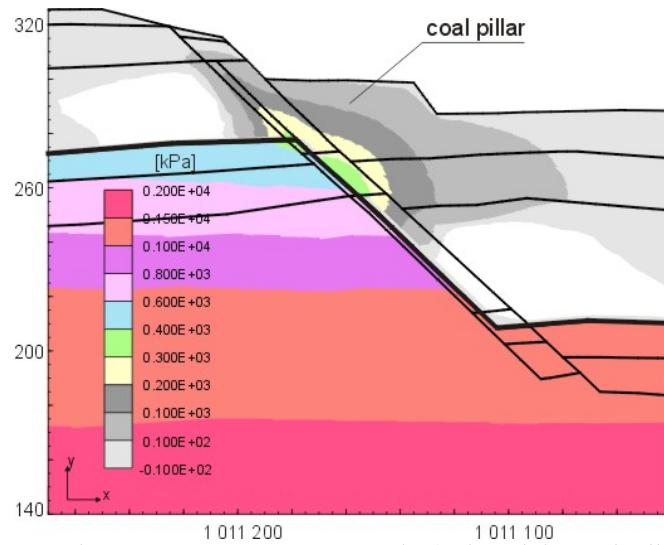


Figure 22a. Leak at Grasset Fault - pore pressure increase in the fault and the coal pillar due to the local hydraulic fracturing of the aquifer confining boundary at the fault.

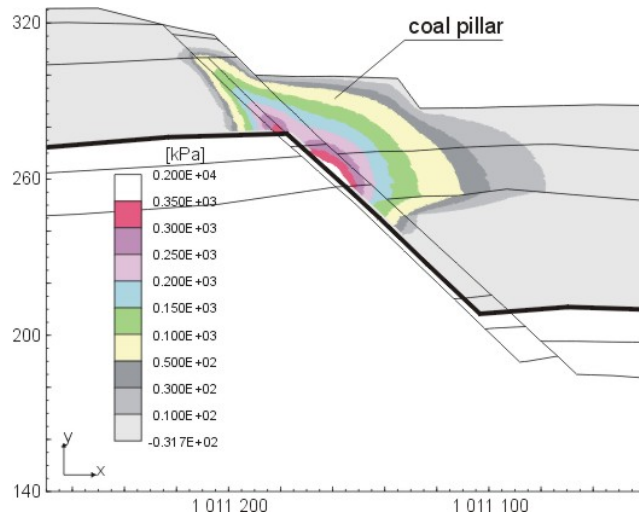


Figure 22b. Leak at Grasset Fault - detail of the pore pressure distribution in the fault and the coal pillar.

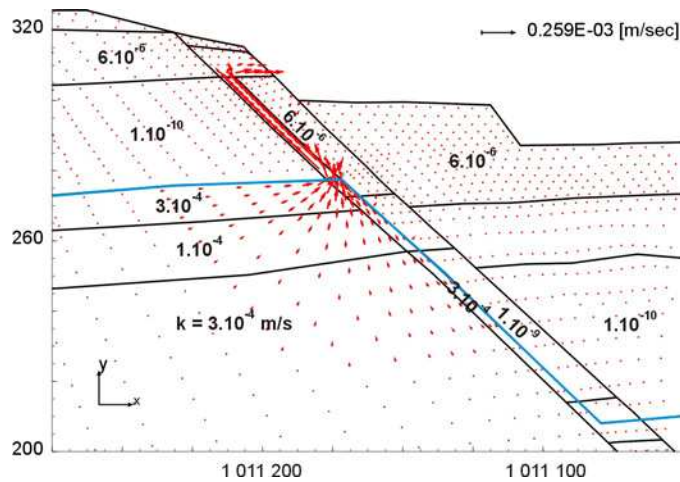


Figure 23. Leak at Grasset Fault - flow rate of the leak at El.306 according to the 2-D model assuming perfectly permeable aquifer.

## CONCLUSIONS

Between 1976 and the present time, safe advance of an open-pit coalmine surcharged by artesian water pressure was successfully controlled through an interactive application of numerical modeling and monitoring. The interactive use of numerical models (calibrated according to field measurements) and a measuring system (updated according to numerical solutions) yielded a synergistic approach that formed a reliable basis for decision-making by regulatory Authorities. The reduction of pressure in a vital regional aquifer and the consequent impact on the surrounding spa region was kept as low as possible, resulting in only smaller consequences with no long-term negative effects on the aquifer. The interactive approach described requires close coordination between the partners concerned with controlling the mining advance and pressure reduction, mapping the geological and hydrogeological conditions, and measuring and modeling the performance of the mine.

## ACKNOWLEDGEMENT

The support of the Grant Agency of the Czech Republic (Grants No 103/97/1053, 103/00/1043 and 103/04/0672) is gratefully acknowledged.

### Appendix. Path Dependent Constitutive Model

#### A1. General Characteristics

A non-linear, path-dependent elastic-plastic (PDEP) model was used in the numerical analyses described in the paper. According to this model (Dolezalova, 1991), the stiffness of the material response depends not only on the stress level, but also on the incremental changes in stress path directions. These are determined by average normal stress level increase/decrease and by relative shear stress level increase/decrease at stress points. A variable stiffness approach is used in the pre-peak regime and a non-associated perfectly plastic approach with a Mohr-Coulomb failure surface in the peak regime. The PDEP model thus approximates the function of other more sophisticated elastic-plastic double hardening models. Although the path-dependent model shows some of the theoretical drawbacks of hypoelastic models, the model—when applied in small increments—accurately describes the deformational response of geomaterials in the pre-peak regime as demonstrated by a great number of numerical analyses for large engineering structures where the PDEP model yielded deformations subsequently confirmed by measurement results.

#### A2. Basic Principles

The basic function of the PDEP model is in compression, and thus we outline the function of the model for the stress states where all the principal stresses are in compression. In Figure 24, the basic stress paths for computation of currently used modulus are labeled with numbers 11, 12, 41 and 42. The first label of the stress path number (1 or 4) indicates increase or decrease of the octahedral normal stress  $\sigma_{oct}$  and the second label of the stress path number (1 or 2) indicates increase or decrease of the shear strength mobilization  $i$ . The assignment of the appropriate stress path results from an evaluation of the change in  $\sigma_{oct}$  and the change in  $i$ . Incremental values  $\Delta\sigma_{oct}$  and  $\Delta i$  are determined for the current and preceding stress states. The procedure of the stress path assignment is depicted in Figure 24. In Figure 24 and in the subsequent description of the PDEP model we use the following notation:

$\sigma_1 \geq \sigma_2 \geq \sigma_3$  - principal stresses (compression is positive);

$\sigma_{iD} = \sigma_i - \sigma_{oct}$  - deviator of the principal stress tensor;

$\sigma_{oct} = \frac{1}{3}(\sigma_1 + \sigma_2 + \sigma_3)$  - octahedral normal stress;

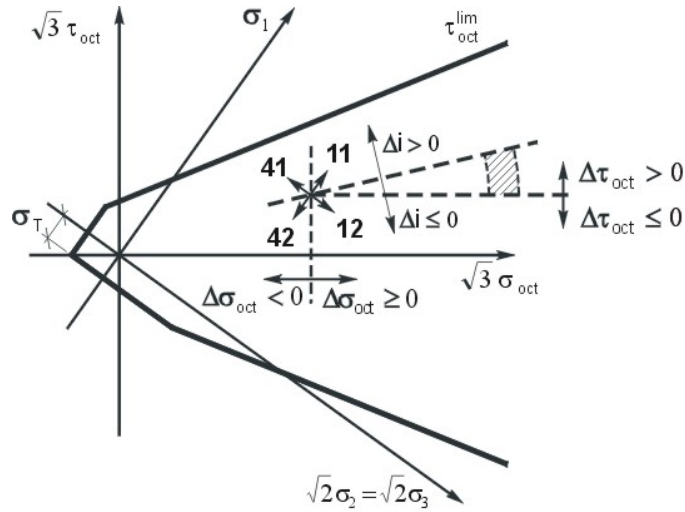
$\sigma_{oct}^{\max}$  - 'historically' maximum value of  $\sigma_{oct}$ ;

$r = \sigma_{oct} / \sigma_{oct}^{\max}$ ;

$\tau_{oct} = \sqrt{\frac{1}{2}(\sigma_{1D}^2 + \sigma_{2D}^2 + \sigma_{3D}^2)}$  - octahedral shear stress;

$\tau_{oct}^{\lim}$  - limit value of octahedral shear stress;

$\sigma_0$  - atmospheric pressure;  
 $\nu_{\max}$  - maximum value of the Poisson ratio;  
 $\nu_p$  - initial value of the tangent Poisson ratio  $\nu_t$  at pressure  $\sigma_0$ ;  
 $k_1, k_2, k_3, p_1$  - exponents fitting the standard triaxial test;  
 $E_{\min} = \delta * E_p$  - minimum permissible modulus;  
 $E_{\max}$  - maximum permissible deformation modulus;  
 $E_p$  - initial value of the tangent deformation modulus  $E_t$  at pressure  $\sigma_0$  (loading modulus);  
 $E_{\text{unl}}$  - unloading modulus;  
 $i = \tau_{\text{oct}} / \tau_{\text{oct}}^{\text{lim}}$  - shear strength mobilization;  
 $i_* = (i - i_0) / (1 - i_0)$  - modified shear strength mobilization;  
 $i_0$  - initial value of shear strength mobilization  $i$ :  $0 < i_0 < 0.20$ ;  
 $\sigma_T$  - tensile strength.



$$i = \frac{\tau_{\text{oct}}}{\tau_{\text{oct}}^{\text{lim}}} \quad i_* = \frac{i - i_0}{1 - i_0} \quad 0 < i_0 < 0.20$$

Figure 24. Graphical representation of the basic stress paths of the PDEP model.

For a given stress path, tangent deformation modulus  $E_t$  and tangent Poisson ratio  $\nu_t$  are computed as follows:

$$\mathbf{11} \quad \underline{\Delta\sigma_{\text{oct}} \geq 0, \Delta i > 0:}$$

$$E_t = E_p \left( \frac{\sigma_{\text{oct}}}{\sigma_0} \right)^{k_1} \left[ 1 - (1 - \delta) i_*^{k_2} \right] \quad (\text{A1})$$

$$\nu_t = \nu_p + (\nu_{\max} - \nu_p) i_*^{k_3} \quad (\text{A2})$$



**12**  $\Delta\sigma_{oct} \geq 0, \Delta i \leq 0$  :

$$E_t = E_p \left( \frac{\sigma_{oct}}{\sigma_0} \right)^{k_1} \quad (\text{A3})$$

$$\nu_t = \nu_p \quad (\text{A4})$$

**41**  $\Delta\sigma_{oct} < 0, \Delta i > 0$  :

$$E_t = E_{unl} [1 - (1 - r)^{p_1}] [1 - (1 - \delta) i_*^{k_2}] \quad (\text{A5})$$

$$\nu_t = \nu_p + (\nu_{\max} - \nu_p) i_*^{k_3}$$

**42**  $\Delta\sigma_{oct} < 0, \Delta i \leq 0$  :

$$E_t = E_{unl} [1 - (1 - r)^{p_1}] \quad (\text{A6})$$

$$\nu_t = \nu_p$$

The basic function of the PDEP model described above is switched off near, or on, the failure surface (e.g.  $0.95 < i < 1.0$ ) and the model then works as a perfectly elastic-plastic model with fixed tangent deformation modulus  $E_t$ .

Checks of minimum and maximum permissible values are performed for each computed  $E_t$  and  $\nu_t$  such that:

$$E_{\min} = \delta E_p \leq E_t \leq E_{\max} \quad (\nu_p \leq \nu_t \leq \nu_{\max})$$

Besides 'basic' stress paths 11, 12, 41 and 42, the PDEP model distinguishes eight additional stress paths that treat cases when at least one of the principal stresses is in tension. These stress paths will not be described here.

### A3. Format of Input Data

We give an example of input data of the PDEP model for the program CRISPATR:

```
### BEGIN EXAMPLE MATERIAL PROPERTIES
C-- PATH DEPENDENT - ELASTIC PLASTIC model no. 9
C-----
C-- CRYSTALLINE ROCK
C--   Ep  NYp  Coh  Fi  Yo  J  Gw  Gs  Kx  Ky  mE  mC
  1 9  3.E6  0.15  1.E3 45.0  0. 4  10.0 25.5 3E-4 3E-4  0.0 0.0
C--   Eunl  Eten  Emax  NYmax  Rten  K1  K2  K3  P1  Delt  Ip  Patm
      10.E6 2.4E6 10.E6 0.40 .5E3 0.01 2.0 2.0 3.0 0.20 0.20 100
C Materials no. 2,3 etc. follow
### END EXAMPLE
```

Material properties of the PDEP model for material No.1 are defined in the above two rows. A comment line is recognized with a sign 'C'. In what follows, we shall describe the meaning of the input values for the two rows of a material:

1st row

|     |   |   |
|-----|---|---|
| 1   | - | material number   |
| 9   | - | ID number of the path dependent elastic-plastic (PDEP) model  |
| Ep  | - | initial value $E_p$ of the tangent deformation modulus $E_t$ [kPa] at pressure $\sigma_{oct}=100$ kPa (loading modulus) |
| NYp | - | initial value $\nu_p$ of the tangent Poisson ratio $\nu_t$ at pressure $\sigma_{oct}=100$ kPa                           |
| Coh | - | cohesion $c$ [kPa]  |



---

|         |   |  |
|---------|---|--|
| Fi      | - | angle of internal friction $\phi$ [°]  |
| Yo      | - | reference value $y_o$ [m] for computation of relative position of a point (only if parameters $E_p$ or $c$ vary with depth, i.e. if $m_E \neq 0$ or $m_C \neq 0$ ) |
| J       | - | yield surface ID number; $J = 4$ is the Mohr-Coulomb yield surface   |
| Gw      | - | unit weight of water $\gamma_w$ [kN/m <sup>3</sup> ]   |
| Gs      | - | total unit weight $\gamma_s$ [kN/m <sup>3</sup> ] (solid and water)  |
| Kx, Ky  | - | permeability coefficient $k_x$ and $k_y$ [m/s] in the horizontal and vertical directions   |
| mE      | - | coefficient $m_E$ for change of the modulus with depth $E_p := E_p + m_E(y_0 - y)$ ; not used for the PDEM model   |
| mC      | - | coefficient $m_C$ for change of cohesion $c$ with depth: $c := c + m_c(y_0 - y)$   |
| 2nd row |   |  |
| Eunl    | - | unloading deformation modulus $E_{unl}$ [kPa]  |
| Eten    | - | deformation modulus in direction of principle tensile stresses $E_{ten}$ [kPa]   |
| Emax    | - | maximum deformation modulus $E_{max}$ [kPa] limiting computed $E_t$ : $E_t \leq E_{max}$   |
| NYmax   | - | maximum Poisson ratio $\nu_{max}$ : $\nu_t \leq \nu_{max}$   |
| Rten    | - | tensile strength [kPa]   |
| K1      | - | exponent $k_1$ governing increase in $E_t$ with increasing $\sigma_{oct}$ ; see Equations (A1) and (A3)  |
| K2      | - | exponent $k_2$ governing decrease in $E_t$ with increasing shear strength mobilization $i_*$ ; see Equations (A1) and (A5)   |
| K3      | - | exponent $k_3$ governing increase in $\nu_t$ with increasing $i_*$ ; see Equation (A2)   |
| P1      | - | exponent $p_1$ governing decrease in $E_{unl}$ with decreasing $r$ ; see Equations (A5) and (A6)   |
| Delt    | - | coefficient $\delta$ governing the minimum value $E_{min} = \delta E_p$ of $E_t$ such that $E_{min} \leq E_t$  |
| Ip      | - | initial value of shear strength mobilization $i_0$   |
| Patm    | - | normalizing atmospheric pressure $\sigma_0$ [kPa]; see Equations (A1) and (A3)   |

#### A4. Open-Pit Coalmine Input Data

The excel datasheet “[IJGCH\\_1\\_1\\_5\\_inputparameters.xls](#)” contains a set of material properties, which have resulted from a trial-and-error fitting procedure as discussed in Section “FEM Code and Constitutive Model” of the paper. This set was used for the Jiri Open-Pit Coalmine numerical analyses without any substantial changes since 1991. Format of the data presented in the worksheet follows the pattern described in Appendix A3 of the paper.

#### REFERENCES

Britto, A. M. & Gunn, M. J. (1987), Critical state soil mechanics via finite elements, Ellis Horwood Ltd., Chichester.

Dolezalova, M. (1986), Deep excavation loaded by artesian water pressure, 8th Danubian European Conference on Soil Mechanics and Foundation Engineering, Vol.1, Nürnberg, pp 247-256.

Dolezalova, M. (1991), Numerical solution of rheological problems, Chapter 12 in Jaroslav Feda: Creep of Soils and Related Phenomena, Academia-Elsevier, pp. 348-385.

Dolezalova, M. et al. (1977), Stability of a deep excavation bottom, Proceedings of 9th International Conference of the International Society for Soil Mechanics and Foundation Engineering, Tokyo, pp. 47-50.

Filip, D. (1975), Stability analysis of the Jiri Mine using physical models from equivalent materials, Research Report, Mining Institute of ASCR, Prague (in Czech).

Hladik, I. (1998), Efficient solution of linear and nonlinear systems of equations for elasticity and elasto-plasticity FEM analyses with unstructured irregular grids, PhD Thesis, University of Innsbruck, Austria.

Hladik, I., Reed, M. B. & Swoboda, G. (1997), Robust preconditioners for linear elasticity FEM analyses, International Journal of Numerical Methods in Engineering, 40, pp. 2109-2127.

Hudek et al. (1986), Final report on geotechnical properties of the coal seam Josef and the volcanic claystone stratum according to in situ tests, Technical Report, PUDIS, Prague (in Czech).

ITASCA Consulting Group, Inc. (1993), Universal Distinct Element Code, Version 2.0, Minnesota, USA.

Pazdera, A. and Vobornikova, H. (1992), Synthesis of geological and hydro-geological conditions of Sokolovsko Coalfield, Technical Report, Geoindustria, Prague (in Czech).

Peck, R. B. (1969), Advantages and Limitations of the Observational Method in Applied Soil Mechanics, Ninth Rankine Lecture, Geotechnique, 19, No 2.

Vobornikova, H. (2003), Personal Communication.



INTERNATIONAL JOURNAL OF  
**GEOENGINEERING  
CASE HISTORIES**

*The Journal's Open Access Mission is  
generously supported by the following Organizations:*



Geosyntec  
consultants

engineers | scientists | innovators

**CONE**TEC



**ENGEO**  
Expect Excellence

Access the content of the ISSMGE International Journal of Geoengineering Case Histories at:  
<https://www.geocasehistoriesjournal.org>